

Photolysis of butenedial at 193, 248, 280, 308, 351, 400, and 450 nm

Yongxin Tang, Lei Zhu *

Wadsworth Center, New York State Department of Health, The Empire State Plaza, Albany, NY 12201-0509, United States
Department of Environmental Health Sciences, State University of New York, Albany, NY 12201-0509, United States

Received 22 February 2005; in final form 27 April 2005
Available online 4 June 2005

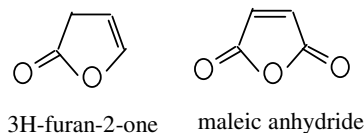
Abstract

We have studied the photolysis of butenedial at 193, 248, 280, 308, 351, 400, and 450 nm by using laser photolysis combined with cavity ring-down spectroscopy. The HCO radical is a photodissociation product at 193 and 248 nm. The corresponding HCO quantum yields are 0.55 ± 0.07 and 0.12 ± 0.01 , independent of butenedial pressure and nitrogen buffer gas pressure. Absorption cross-sections of butenedial are $(6.88 \pm 0.39) \times 10^{-18}$ and $(3.62 \pm 0.69) \times 10^{-19}$ cm² at 193 and 248 nm. The end-products from the photolysis of butenedial at 193, 248, 308, and 351 nm were measured by FTIR. Acrolein and 3H-furan-2-one were observed and their yields have been estimated.

© 2005 Elsevier B.V. All rights reserved.

1. Introduction

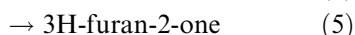
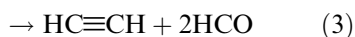
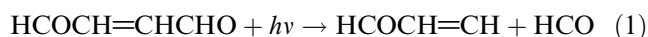
Butenedial (HCOCH=CHCHO), the simplest unsaturated dialdehyde, is a ring-cleavage product formed from photochemical oxidation of aromatic hydrocarbons [1–5]. Photolysis and reactions with OH, O₃, and NO₃ are its possible tropospheric removal pathways [6]. The OH/butenedial reaction rate constants have been measured by Bierbach and coworkers [7] using the relative rate technique. They were $(5.2 \pm 0.1) \times 10^{-11}$ and $\geq (2.4 \pm 0.8) \times 10^{-11}$ cm³ molecule⁻¹ s⁻¹ for *cis*- and *trans*-butenedial. Bierbach and coworkers [7] concluded that although OH radical reaction is an important atmospheric sink for butenedial, its photolysis will probably be an even stronger sink. In addition to *trans/cis* isomerization product which accounted for $\leq 40\%$ of butenedial decay, the major product formed from visible lamp (320–480 nm) irradiation of *cis*- and *trans*-butenedial mixture in air was 3H-furan-2-one (cyclic-C₄H₄O₂). The minor product was maleic anhydride (cyclic-C₄H₂O₃).



When a UV lamp (254 nm) was used to irradiate *cis*- and *trans*-butenedial mixture in air, the major products observed were maleic anhydride and 3H-furan-2-one along with $\sim 45\%$ *trans/cis* isomerization product [7]. The minor product observed was acetylene. However, Bierbach and coworkers were not able to obtain absolute photolysis product yields, since the butenedial concentration was not accurately known due to the presence of impurities in their samples. With the use of an improved method to produce butenedial, Liu and coworkers [6] were able to produce butenedial with purity $\geq 90\%$. They studied OH- and O₃-initiated photooxidations of butenedial in a smog chamber and reported O₃/butenedial reaction rate constant of $(1.6 \pm 0.1) \times 10^{-18}$ cm³ molecule⁻¹ s⁻¹. Liu and coworkers did not observe anhydride from butenedial photolysis, but they did detect a very small amount of acrolein (CH₂=CHCHO). The solution-phase UV absorption spectrum of butenedial has been measured

* Corresponding author. Fax: +1 518 473 2895.
E-mail address: zhul@wadsworth.org (L. Zhu).

in the 290–490 nm region [8], but its gas-phase UV absorption spectrum has not been reported. Product channels and quantum yields following gas-phase photolysis of butenedial and their wavelength dependencies are not well known. Such information is needed in order to estimate the radical- and oxidant-formation capabilities of butenedial and to elucidate the atmospheric fates of aromatic hydrocarbons. Photolysis of butenedial can occur via the following pathways:



Photolysis channels (1)–(3) are radical-formation channels. Photolysis channels (4) and (5) are molecular-elimination and photocyclization channels. In order for $\text{HCOCH}=\text{CH} + \text{HCO}$ to be formed from butenedial photolysis, a C–C bond, which is a part of the conjugated π system ($\text{O}=\text{C}-\text{CH}=\text{CH}-\text{C}=\text{O}$), needs to be broken. In the absence of the heats of formation for butenedial and its photolysis products, the threshold wavelength for the formation of $\text{HCOCH}=\text{CH} + \text{HCO}$ from butenedial photolysis is expected to be shorter than the calculated photochemical threshold [9,10] of ~ 340 nm for the formation of R + HCO products from the photolysis of saturated aliphatic aldehydes.

In this Letter, we report results obtained from an experimental study of the photolysis of butenedial at 193, 248, 280, 308, 351, 400, and 450 nm by using laser photolysis combined with the cavity ring-down technique [11,12]. The HCO radical was only observed at photolysis wavelengths of 193 and 248 nm; the corresponding HCO quantum yields have been measured. The end-products (acrolein and 3H-furan-2-one) from the photolysis of butenedial at 193, 248, 308, and 351 nm have been identified with FTIR, and their corresponding yields have been estimated.

2. Experimental technique

The experimental setup has been described in detail elsewhere [9,10,13]. An excimer or a dye laser was used to photolyze butenedial, while a nitrogen-pumped dye laser was used to probe the HCO radical product. The photolysis radiation at 193, 248, 308, and 351 nm was provided by an excimer laser, while that at 280, 400, and 450 nm was provided by either the fundamental or the second harmonic output of an excimer pumped dye laser. Laser dyes used were coumarin 153, furan 2, and coumarin 2. The reaction cell was vacuum-sealed with a pair of high-reflectance cavity mirrors. The

photolysis beam entered the reaction cell at a 15° angle to the main cell axis through a sidearm. The probe laser beam was directed along the main optical axis of the cell and it overlapped spatially with the photolysis beam at the center of the reaction cell. A fraction of the probe laser pulse was injected into the cavity through the front mirror and its intensity decay inside the cavity was measured by monitoring the weak transmission of light through the rear mirror with a photomultiplier tube (PMT). The PMT output was amplified, digitized, and sent to a computer. The decay curve was fitted to a single-exponential decay function from which the ring-down time constant and the total loss per optical pass were calculated. By measuring the cavity losses with and without a photolysis pulse, we obtained the HCO absorption from the photolysis of butenedial. A pulse/delay generator was used to vary the delay time between the firing of the photolysis and the probe lasers. Quantum yield measurements were made at a laser repetition rate of 0.1 Hz, to ensure the replenishment of the gas samples between successive photolysis pulses. The spectrum scan was performed at a laser repetition rate of 1 Hz. All experiments were carried out at an ambient temperature of 293 ± 2 K. The stable end-products from the photolysis of butenedial were characterized by a Fourier transform infrared spectrometer connected on-line with the photolysis cell.

Butenedial was synthesized using literature methodology [8,14,15]. A solution of bromine in methanol was added dropwise to a solution of freshly distilled furan in methanol at -78°C under an argon atmosphere. The orange-colored reaction mixture was stirred for about 2.5 h at -10°C and a pale yellow solution formed. Powdered anhydrous Na_2CO_3 was subsequently added to quench the reaction. The resulting mixture was stirred at room temperature overnight, followed by addition of ether and removal of the solid by filtration. After the solvent was removed at reduced pressure, the residue was purified by vacuum distillation, and 1,1,4,4-tetramethoxy-2-butene was collected. Amberlyst-15 was added to a solution of 1,1,4,4-tetramethoxy-2-butene in acetone and water. The resulting mixture was stirred at room temperature at least overnight. The solid was filtered out and aqueous residue was extracted with CH_2Cl_2 and washed with brine. The organic layers were dried over Na_2SO_4 and the solvent was removed. Butenedial was collected by immersion of the receiver end of the vacuum distillation in a bath at -78°C [15]. *trans*-Butenedial was a solid, while *cis*-butenedial was a liquid at room temperature. The collected sample was a yellow mixture of *cis*- and *trans*-butenedial. Before each experiment, the sample was further purified by repeated freeze–pump–thaw cycles at -78°C ; this removed volatile impurities. The purity of the butenedial sample was checked with H-NMR and was $\geq 90\%$.

Formaldehyde was generated by the pyrolysis of paraformaldehyde ($\geq 95\%$ purity, Aldrich) at 110 °C. CCl_4 ($\geq 99.9\%$ purity, Aldrich) was purified by repeated freeze–pump–thaw cycles. Nitrogen ($\geq 99.999\%$ purity, BOC Edwards) was used without further purification.

3. Results and discussion

3.1. Time-resolved studies of butenedial photolysis at 193, 248, 280, 308, 351, 400, and 450 nm

3.1.1. General features

We have studied the photolysis of butenedial at 193, 248, 280, 308, 351, 400, and 450 nm and only observed the HCO radical at photolysis wavelengths of 193 and 248 nm. The lack of HCO product from the butenedial photolysis in the 280–450 nm region suggests that the photolysis of unsaturated dialdehyde is very different from the photolysis of saturated dialdehydes such as glyoxal ($(\text{CHO})_2$). Our group reported [16] the HCO radical quantum yields from the photolysis of glyoxal in the 290–420 nm region: these were 0.50 ± 0.01 , 0.84 ± 0.07 , 1.34 ± 0.06 , 2.01 ± 0.08 , 0.74 ± 0.08 , and 0.48 ± 0.03 at 290, 310, 350, 390, 400, and 420 nm, respectively. The lack of HCO product from the photolysis of butenedial at 280 and 308 nm also suggests that the photolysis of unsaturated dialdehyde is different from the photolysis of saturated aliphatic aldehydes. The threshold wavelength for the formation of $\text{HCOCH}=\text{CH} + \text{HCO}$ from the photolysis of butenedial is expected to be shorter than that for the photolysis of the saturated aliphatic aldehydes (~ 340 nm), because a C–C bond in the conjugated π system ($\text{O}=\text{C}-\text{C}=\text{C}-\text{C}=\text{O}$) needs to be broken. The thermochemistry of the process $\text{HCOCH}=\text{CHCHO} \rightarrow \text{HCOCH}=\text{CH} + \text{HCO}$ is estimated to be around $98\text{--}99 \text{ kcal mol}^{-1}$ from the NIST database estimation method and assuming the same C–H bond dissociation energy for the vinylic C–H bond in acrolein as that in ethene ($110 \text{ kcal mol}^{-1}$). This corresponds to an estimated photochemical threshold of about 290 nm for the formation of $\text{HCOCH}=\text{CH} + \text{HCO}$ from butenedial photolysis. Other reasons for the lack of observable HCO signal from the photolysis of butenedial in the 280–450 nm region are the much smaller butenedial absorption cross-sections ($< 6 \times 10^{-21} \text{ cm}^2$) at these wavelengths and the low room temperature vapor pressure of butenedial (~ 1.4 Torr). The absorption cross-sections of butenedial at 193 and 248 nm have been determined in this study to be $(6.88 \pm 0.39) \times 10^{-18}$ and $(3.62 \pm 0.69) \times 10^{-19} \text{ cm}^2$, respectively. Thus, the magnitude of the gas phase UV absorption cross-sections of butenedial at 193 and 248 nm are at least 1146 and 60 times those in the 280–450 nm region. Hufford and coworkers [15] measured the UV absorption spectrum of butenedial in *i*-octane solution in the 220–500 nm re-

gion and observed two absorption bands. One peaked at 225 nm ($\epsilon = 17000$) and the other peaked at 354 nm ($\epsilon = 70$). Thus, the results from the present gas phase study and the previous aqueous phase study suggest that there are two absorption bands of butenedial in the UV/visible region with the band at shorter wavelength region being much stronger than the band at longer wavelength region. Certainly, the UV/visible absorption spectrum of butenedial is distinctly different from that of a saturated dialdehyde such as glyoxal. Glyoxal displays two absorption bands above 220 nm in the UV/visible region with the longer wavelength band (peaking at 455 nm with σ of $4.7 \times 10^{-19} \text{ cm}^2$) being much stronger than the shorter wavelength band (peaking at 299 nm with σ of $3.96 \times 10^{-20} \text{ cm}^2$) [17–19].

3.2. HCO radical quantum yields from the photolysis of butenedial at 193 and 248 nm

Presented in Fig. 1 is a cavity ring-down absorption spectrum of the product after 193 nm photolysis of butenedial and a previously reported absorption spectrum of HCO in the same wavelength region [20]. The similarity between these two spectra indicates that the HCO radical is a photolysis product of butenedial. A similar product absorption spectrum was obtained at a photolysis wavelength of 248 nm. The cavity ring-down spectrometer was tuned to the $\text{HCO X}^2\text{A}''(0,0,0) \rightarrow \text{A}^2\text{A}'(0,9,0)$ R bandhead at 613.8 nm and the HCO absorption after the photolysis of butenedial was determined. The HCO radical quantum yields from butenedial photolysis were determined from the ratio of the HCO concentration produced in the pump/probe laser overlapping region to the absorbed photon density in the same region. The overlapping region could be viewed as a rectangular solid with its width and height defined by the dimensions of the photolysis beam and the length of the rectangular solid defined by $(\text{beam width}) \times (\tan 15^\circ)^{-1}$, where 15° is the crossing angle between the pump and the probe laser beams. The absorbed photolysis photon density in the pump/probe laser overlapping region could be derived from the difference between the transmitted photolysis beam energies entering (E_{in}) and leaving (E_{out}) that region, the individual photon energy (hc/λ) at the photolysis wavelength (λ), and the volume (v) of the overlapping region via the following equation:

$$\text{Absorbed photon density} = \frac{E_{\text{in}} - E_{\text{out}}}{h(c/\lambda)v}.$$

The photolysis beam energy entering or leaving the photolysis/probe laser overlapping region can be calculated from the incident photolysis beam energy entering the cell (E_0), the absorption cross-section (σ) and the density (n) of butenedial in the cell, and the absorbing path length, by application of Beer's law:

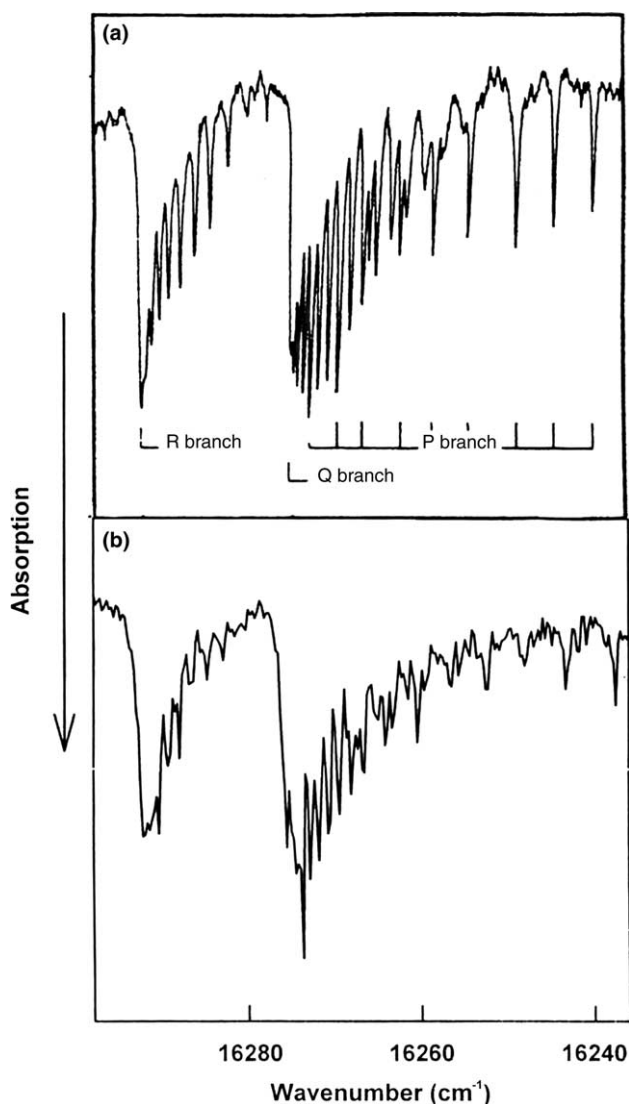


Fig. 1. (a) Intracavity laser absorption spectrum of HCO following photolysis of CH_3CHO at 266 nm (adapted from [20]). (b) Cavity ring-down absorption spectrum of the product from the photolysis of butenedial at 193 nm.

$$E_{\text{in}} = E_0 \cdot \exp(-\sigma n l_1),$$

$$E_{\text{out}} = E_0 \cdot \exp(-\sigma n l_2),$$

where l_1 is the distance between the photolysis beam entrance and the beginning of the pump/probe laser overlapping region, and l_2 is the distance between the photolysis beam entrance and the end of the pump/probe laser overlapping region. The incident photolysis beam energy was measured by a calibrated joulemeter placed in front of the cell. The incident beam energy inside the cell was corrected for transmission loss at the front cell window, and for reflection of the photolysis beam from the rear cell window. The absorption cross-section of butenedial was obtained by monitoring the transmitted photolysis photon intensity as a function of butenedial pressure in the cell, and by applying Beer's

law to the experimental data. The absorption cross-sections of butenedial thus obtained were $(6.88 \pm 0.39) \times 10^{-18}$ and $(3.62 \pm 0.69) \times 10^{-19} \text{ cm}^2$ at 193 and 248 nm, respectively. Error bars quoted (1σ) give the estimated precision of cross-section determination: this includes the standard deviation for each measurement plus the standard deviation about the mean of 15 repeated experimental runs at 193 nm and 12 repeated experimental runs at 248 nm. The HCO concentration after the photolysis was obtained by measurement of its absorption at 613.80 nm at a photolysis and a probe laser delay of 15 μs . The absolute HCO radical concentration following 193 nm photolysis of butenedial was calibrated relative to that obtained from the $\text{Cl} + \text{H}_2\text{CO}$ reaction, using 193 nm photolysis of CCl_4 as chlorine atom precursor. The HCO concentration from 248 nm photolysis of butenedial was calibrated relative to formaldehyde photolysis at 248 nm, for which the recommended HCO quantum yield is available [21]. The dependence of the HCO quantum yields on butenedial pressure and nitrogen buffer gas pressure (2–260 Torr) was examined; no dependence was observed. The HCO quantum yields from the photolysis of butenedial at 193 and 248 nm are 0.55 ± 0.07 and 0.12 ± 0.01 , where errors quoted (1σ) are the estimated precision of quantum yield measurements. Systematic errors contain uncertainties in the determination of the HCO absorption cross-section ($\sim 20\%$), butenedial concentration and absorption cross-section ($\sim 11\%$ at 193 nm, and $\sim 24\%$ at 248 nm), pulse energy ($\sim 5\%$), and the angle between the photolysis and the probe lasers (3%). When relative and systematic errors are summed, the overall uncertainty in the determination of HCO quantum yields is about 52% at 193 nm, and about 60% at 248 nm.

3.3. Photolysis end-product studies with FTIR at 193, 248, 308, and 351 nm

Butenedial ($n_{\text{butenedial}} \sim 0.97 \times 10^{16} \text{ molecules cm}^{-3}$) was photolyzed in a closed cell by excimer laser operating at 193, 248, 308, and 351 nm. The photolysis end-products were transferred to a 10-m White cell and were analyzed by an FTIR. Presented in Fig. 2 are FTIR spectra of butenedial with (7200 photolysis pulses for duration of 2 h) and without 308 nm photolysis and the corresponding amplified differential spectrum. The negative absorption bands in the differential IR spectrum at 1060 cm^{-1} and in the $1702\text{--}1745 \text{ cm}^{-1}$ region correlate with those of dissociated butenedial. The IR absorption bands in the 920–958, 1157–1166, 1411–1428, 1800–1860, $2040\text{--}2250 \text{ cm}^{-1}$ (CO), and $2280\text{--}2380 \text{ cm}^{-1}$ (CO_2) regions increase in intensity after the photolysis. CO_2 is probably an artifact resulting from reactions at the wall of the cell. The IR absorption bands at 920–958, 1157–1166, and 1411–1428 cm^{-1} correlate with those of acrolein formed from butenedial

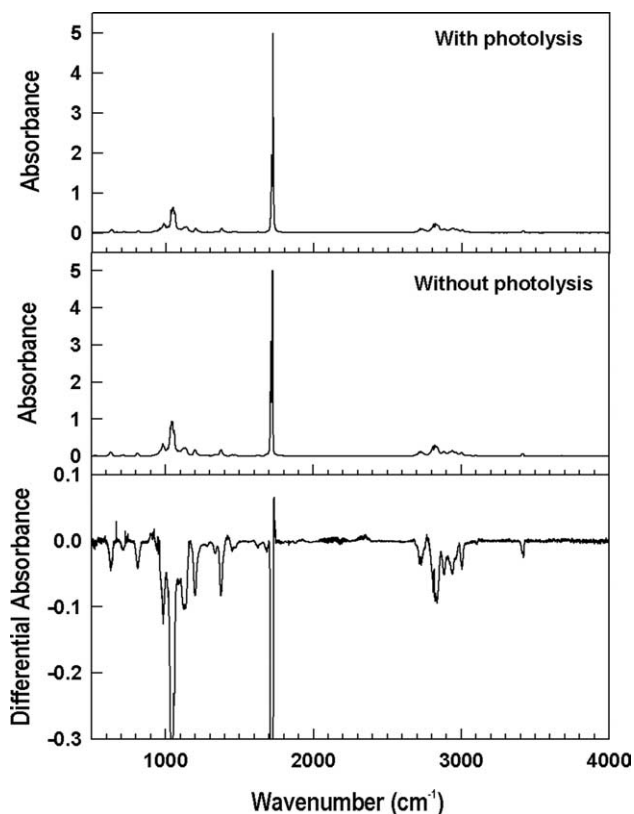
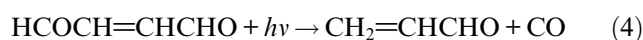
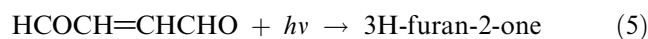


Fig. 2. FTIR spectra of butenedial with and without photolysis radiation at 308 nm and the corresponding amplified differential FTIR spectrum. The butenedial pressure in the reaction cell was 0.3 Torr. When the reaction cell was open to the White cell in the absence of photolysis, the equilibrated butenedial pressure was 0.16 Torr.

photolysis (a comparison of the butenedial photolysis product spectrum with that of acrolein in the 1395–1441 cm^{-1} region is given in Fig. 3):



The IR absorption band in the 1800–1860 cm^{-1} region and peaking sharply at 1834 cm^{-1} correlates with that of 3H-furan-2-one formed from butenedial photolysis (a comparison of the butenedial photolysis product spectrum in the 1800–1860 cm^{-1} region with that of 3H-furan-2-one is given in Fig. 3):



CO is probably a product of the $\text{HCOCH}=\text{CH} + \text{HCO}$, $\text{CH}_2=\text{CHCHO} + \text{CO}$, and $\text{HC}\equiv\text{CH} + 2\text{HCO}$ product channels and a secondary product from the photolysis of acrolein. From the IR spectra of butenedial with and without photolysis, and using sample standards to calibrate the product IR spectra, we obtained estimated yields of acrolein and 3H-furan-2-one from the photolysis of butenedial at 193, 248, 308, and 351 nm and they are listed in Table 1. The respective acrolein quantum yields which were determined relative to the loss of the starting material are about 1.1%, 3.7%, 15%, and 23%

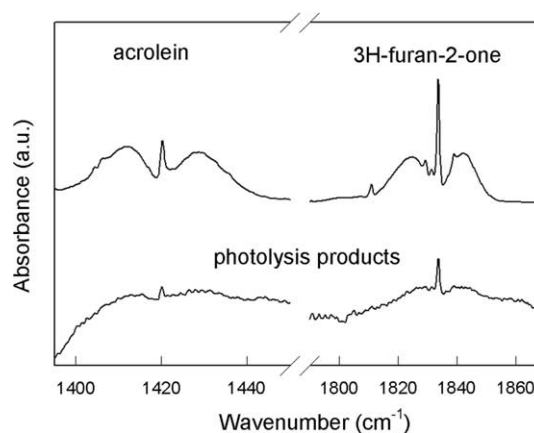


Fig. 3. A comparison of the butenedial photolysis product spectra in the 1395–1441 and 1800–1860 cm^{-1} region (obtained by expanding the photolysis product spectrum shown in Fig. 2 and subtracting the contribution of the starting material) with those of acrolein and 3H-furan-2-one standard.

at 193, 248, 308, and 351 nm. Since acrolein formed from the photolysis of butenedial in a closed cell with many laser pulses can also be photolyzed by excimer laser radiation at 193, 248, 308, and 351 nm [22–24], the acrolein yields reported here are the estimated minimum. 3H-furan-2-one was only observed from the photolysis of butenedial at 248, 308, and 351 nm; the corresponding estimated minimum product yields were about 2.8%, 1.2%, and 1.1%. Due to the complex secondary chemistry involved and multiple channels were responsible for CO production, we were not able to obtain channel-specific CO yields. Liu and coworkers [6] detected a very small amount of acrolein when photolyzing butenedial in a smog chamber, but they did not report product quantum yield. Bierbach and coworkers [7] studied the photolysis of a mixture of *cis*- and *trans*-butenedial in air using visible lamp irradiation (320–480 nm). In addition to *trans/cis* isomerization product which accounted for $\leq 40\%$ of butenedial decay, the major product observed was 3H-furan-2-one (cyclic- $\text{C}_4\text{H}_4\text{O}_2$), and the minor product observed was maleic anhydride (cyclic- $\text{C}_4\text{H}_2\text{O}_3$). When Bierbach and coworkers [7] used a UV lamp (254 nm) to irradiate *cis*- and *trans*-butenedial mixture in air, the major photolysis products that they observed were maleic anhydride and 3H-furan-2-one, along with $\sim 45\%$ *trans/cis* isomerization product. Bierbach and coworkers [7] also observed acetylene as a minor product. However, they were not able to obtain absolute photolysis product yields, since they were not able to produce pure butenedial. Although we observed 3H-furan-2-one from the photolysis of butenedial at 248, 308, and 351 nm, it was a minor photolysis product as compared with acrolein. We did not observe maleic anhydride as a butenedial photolysis product, since our end-product study

Table 1
Absorption cross-sections of butenedial and its photolysis product yields

| Wave (nm) | σ (butenedial, cm^2) | ϕ_{HCO} | ϕ_{acrolein} (%) | $\phi_{\text{3H-furan-2-one}}$ (%) |
|-----------|---------------------------------------|---------------------|------------------------------|------------------------------------|
| 193 | $(6.88 \pm 0.39) \times 10^{-18}$ | 0.55 ± 0.07 | ≥ 1.1 | 0 |
| 248 | $(3.62 \pm 0.69) \times 10^{-19}$ | 0.12 ± 0.01 | ≥ 3.7 | ≥ 2.8 |
| 308 | $< 6 \times 10^{-21}$ | 0 | ≥ 15 | ≥ 1.2 |
| 351 | $< 6 \times 10^{-21}$ | 0 | ≥ 23 | ≥ 1.1 |

was done in the absence of air. We have observed acetylene from the photolysis of butenedial only at 193 nm with an estimated yield of $\sim 42\%$.

3.4. Atmospheric implications

Since the absorption cross-sections of butenedial are small in the actinic UV region and since the photolysis of butenedial does not lead to the formation of HCO radical in this wavelength region, butenedial photolysis is not an important source of radicals in the atmosphere. The quantum yield of acrolein is significant from butenedial photolysis in the actinic UV region. Thus, butenedial photolysis can be a significant source of acrolein in the atmosphere.

Acknowledgments

Discussions with Mr. Chaomin Li and Dr. Yunqing Chen about butenedial synthesis are acknowledged. We thank Dr. Lynn McNaughton at the NMR Core Facility of the Wadsworth Center for performing H-NMR characterization of the butenedial samples. We are grateful for the support provided by the National Science Foundation under Grant ATM-0300294.

References

- [1] K.-H. Becker, I. Barnes, A. Bierbach, K.J. Brockmann, F. Kirchner, B. Klotz, H.G. Libuda, A. Mayer-Figge, S. Mönninghoff, L. Ruppert, W. Thomas, E. Wiesen, K. Wirtz, F. Zabel, in: G. Le Bras (Ed.), *Chemical Processes in Atmospheric Oxidation*, Springer, Berlin, 1997, p. 79.
- [2] J. Yu, H.E. Jeffries, *Atmos. Environ.* 31 (1997) 2261.
- [3] F. Motta, G. Ghigo, G. Tonachini, *J. Phys. Chem. A* 106 (2002) 4411.
- [4] P.B. Shepson, E.O. Edney, E.W. Corse, *J. Phys. Chem.* 88 (1984) 4122.
- [5] B.E. Dumdei, R.J. O'Brien, *Nature* 311 (1984) 248.
- [6] X. Liu, H.E. Jeffries, K.G. Sexton, *Environ. Sci. Technol.* 33 (1999) 4212.
- [7] A. Bierbach, I. Barnes, K.H. Becker, E. Wiesen, *Environ. Sci. Technol.* 28 (1994) 715.
- [8] X. Liu, Ph.D. Thesis, University of North Carolina, Chapel Hill, NC, 1999.
- [9] T.J. Cronin, L. Zhu, *J. Phys. Chem. A* 102 (1998) 10274.
- [10] Y. Tang, L. Zhu, *J. Phys. Chem. A* 108 (2004) 8307.
- [11] A. O'Keefe, D.A.G. Deacon, *Rev. Sci. Instrum.* 59 (1988) 2544.
- [12] A. O'Keefe, J.J. Scherer, A.L. Cooksy, R. Sheeks, J. Heath, R.J. Saykally, *Chem. Phys. Lett.* 172 (1990) 214.
- [13] L. Zhu, G. Johnston, *J. Phys. Chem.* 99 (1995) 15114.
- [14] D. Frederico, P.M. Donate, M.G. Constantino, E.S. Bronze, M.I. Sairre, *J. Org. Chem.* 68 (2003) 9126.
- [15] D.L. Hufford, D.S. Tarbell, T.R. Koszalka, *J. Am. Chem. Soc.* 74 (1952) 3014.
- [16] Y. Chen, L. Zhu, *J. Phys. Chem. A* 107 (2003) 4643.
- [17] A. Horowitz, R. Meller, G.K. Moortgat, *J. Photochem. Photobiol. A* 146 (2001) 19.
- [18] C.N. Plum, E. Sanhueza, R. Atkinson, W.P.L. Carter, J.N. Pitts Jr., *Environ. Sci. Technol.* 17 (1983) 479.
- [19] J.J. Orlando, G.S. Tyndall, *Int. J. Chem. Kinet.* 33 (2001) 149.
- [20] F. Stoeckel, M.D. Schuh, N. Goldstein, G.H. Atkinson, *Chem. Phys.* 95 (1985) 135.
- [21] R. Atkinson, D.L. Baulch, R.A. Cox, R.F. Hampson Jr., J.A. Kerr, J. Troe, *J. Phys. Chem. Ref. Data* 21 (1992) 1125.
- [22] I. Magneron, R. Thévenet, A. Mellouki, G. Le Bras, G.K. Moortgat, K. Wirtz, *J. Phys. Chem. A* 106 (2002) 2526.
- [23] E.P. Gardner, P.D. Sperry, J.G. Calvert, *J. Phys. Chem.* 91 (1987) 1922.
- [24] J.W. Coomber, J.N. Pitts Jr., *J. Am. Chem. Soc.* 91 (1969) 547.